Journal of Information Hiding and Multimedia Signal Processing ©2016 ISSN 2073-4212
Ubiquitous International Volume **7**, Number **1**, January **2016**

Multifocus Image Fusion by Sum of Local Variance Energy

Peng Geng

School of Information Science and Technology
Shijiazhuang Tiedao University
No.17,Beierhuan East Road,Shijiazhuang, China
Gengpeng@stdu.edu.cn

Song Tian

General Education Institute
Beijing International Studies University

Kai Lu

School of Information Science and Technology
Shijiazhuang Tiedao University
No.17,Beierhuan East Road,Shijiazhuang, China

Received March, 2015; revised November, 2015

Abstract. *An effective multifocus image fusion method is presented for creating a highly informative fused image through merging multiple source images. Based on the nonsubsampled contourlet transform, the new multiscale geometry analysis of MNSDFB (Combining Multiwavelet and Nonsubsampled direction filter bank) transform is proposed to decompose the source multifocus images. Firstly, in the proposed image fusion scheme, the source images are decomposed to different directions coefficient in every scale by the presented MNSDFB transform. Secondly, the sum of local variance energy is proposed as the focus metric of every direction coefficient. Finally, the merged coefficients are reconstructed by the inverse MNSDFB transform. The proposed scheme is compared with the state-of the-art methods on the four pair of multifocus images. The subjective and objective performance demonstrated that the proposed scheme is effective in merging the multifocus images.*
Keywords: Mage fusion, Local variance, Multiwavelet, NSDFB.

1. **Introduction.** Image fusion is the process of merging information from two or more images of the same scene so that the resulting image will be more suitable for human and machine perception or further image processing tasks such as automatic target recognition, computer vision, remote sensing, robotics, complex intelligent manufacturing, medical image processing, and military purposes. A better image fusion method can merge the useful information of source images and introduce little of artifacts in the fused images. Many multifocus fusion algorithms have been proposed in recent years. Basically, these fusion algorithms can be categorized into two groups: spatial domain fusion and transform domain fusion. The common algorithms in spatial domain include average, variance, energy of image gradient, sum modified Laplacian, and spatial frequency [1-2]. On the other hand, there are many kinds of transform domain including principal component

analysis (PCA)[3], pyramid, wavelet [4], curvelet [5], contourlet [6], and nonsubsampled contourlet transform (NSCT) [7], shearlet [8], etc. Owing to good localized time frequency characteristics of discrete wavelet transform (DWT), Yang et al.[9] proposed the maximum sharpness focus measure and neighbor energy to select low and high frequency subbands coefficients in DWT domain. However, the limitations of wavelet direction make it does not perform well multidimensional data such as image. Liu [10] adopted the cycle spinning to overcome lack of shift-variance in contourlet transform and subsequently merge the multifocus images. The fractional differential and NSCT is proposed to fuse multifocus images by Zhong [11]. Traditional regional energy and multiple regional features are used to fuse the low frequency shearlet coefficients and high frequency shearlet coefficients [12]. These new MSD theory provide higher directional sensitivity than wavelets. However, some artifacts in the image edges appear to some degree because the curvelet, bandelet and contourlet are short of translation-invariance. Furthermore, the redundancy in shearlet and NSCT decomposition makes the run-time very slow in image processing including image fusion, although the shearlet and NSCT can capture the point discontinuities of image and track the curve directions of images. Inspired by the construction of NSCT in [7] which combines the nonsubsampled laplacian transform with the nonsubsampled directional filter bank (NSDFB), we propose a new image multiresolution and multiscale representation method which combines the Multiwavelet transform with NSDFB called as MNSDFB transform in this paper. Besides the MNSDFB, the sum of local variance energy rule is introduced to merge the coefficient of the proposed MNSDFB decomposition.The presented method is compared with other fusion methods such as multiresolution singular value decomposition, nonsubsampled contourlet transform, and cross bilateral filter.

2. **Related works.**

2.1. **Multiwavelet.** Goodman firstly constructed the multiwavelet in 1994 [13]. G. Donovan applies the fractal interpolation approach to reconstructing the Geronimo, Hardin and Massopust (GHM) multiwavelet whose support basis is in [0 2] [14]. Multiwavelet has the property of orthogonality, symmetry, high approximation, and good regularity. Both multiwavelet and scalar wavelet are based on multiscale geometry analysis theory. Multiwavelet is composed of the scale function$\Phi(t) = [\phi_1(t), \phi_2(t)...\phi_r(t)]^T$ and the wavelet function $\Psi(t) = [\psi_1(t), \psi_2(t)...\psi_r(t)]^T$ after translation and expansion [15]. The multiwavelet two-scale equations verified the following:

$$\Phi(t) = \sqrt{2}\sum_{k=0}^{L} H_k \Phi(2t-k) \qquad k \in Z \tag{1}$$

$$\Psi(t) = \sqrt{2}\sum_{k=0}^{L} G_k \Psi(2t-k) \qquad k \in Z \tag{2}$$

Where l is the number of scaling coefficients and H_k and G_k are the lowpass and highpass matrix filter for each translation distance k, respectively. There are r ($r = 2$) scaling function in the multiwavelet transform. Similar to traditional wavelet, the decomposition and reconstruction of Multiwavelet is as follows:

$$S_{j-1,n} = \sum_k H_{k-2n} \cdot S_{j,k} \cdot d_{j-1,n} = \sum_k G_{k-2n} \cdot S_{j,k} \tag{3}$$

$$S_{j,n} = \sum_k H^*_{k-2n} \cdot S_{j-1,k} + \sum_k G^*_{k-2n} \cdot d_{j-1,n} \tag{4}$$

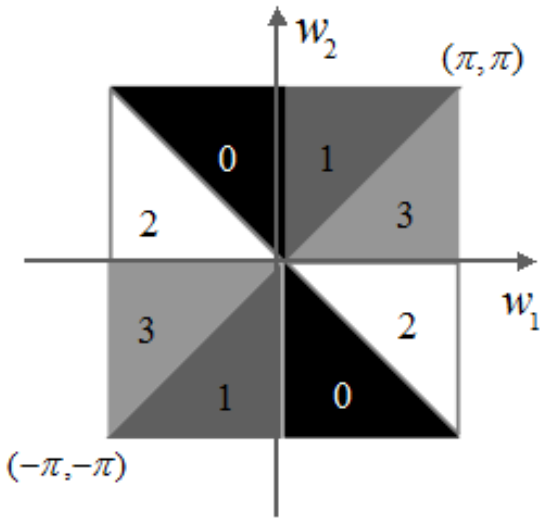

FIGURE 1. Frequency partitioning of four-channel directions NSDFB.

Where $S_{j-1,n}$ is the r dimension low frequency component. $d_{j-1,n}$ stands for r dimension high frequency component. * is the conjugate and transpose operation.

2.2. **NSDFB.** Nonsubsampled direction filter bank (NSDFB) is a new kind filter bank used in the nonsubsampled contourlet transform. There are two modules of the two-channel quincunx filter banks and the shearing operation in the NSDFB. The 2-D images can be divided into horizontal directions and vertical direction by the two-channel quincunx filter banks. The second module is executed before the end of the decomposition of quincunx filtering, and after the composite phase, it conducts an anti-shearing operation. Its function is reordering the image sampling. Actually, the shearing operation is a kind of image sampling. After this operation, the image is revolved and the width becomes twice wider than before. The key of NSDFB is that it combines the shearing operation with the quincunx filter banks in the points of tree-structure. To achieve multidirection decomposition, the NSDFB is iteratively used. Fig.[1] illustrates a four-channel directional decomposition.

2.3. **The MNSDFB Transform.** Other than the NSCT, the transform of the multiwavelet combining with the NSDFB, named as MNSDFB transform, is presented. An image is firstly decomposed into a lowpass subband and three highpass subbands by the multiwavelet transform. Every subband is subsequently decomposed into several directional subbands by the NSDFB. In this paper, the two levels decomposition of the multiwavelet is used. After that, every subband of multiwavelet is decomposed to four directions by the NSDFB. The MNSDFB decomposition process can clearly be described in the Fig.2.

3. **Proposed Fusion Rule.** Human visual system is sensitive to the high frequency part of image which is relative to the detail information of an image. Therefore, similar to structural similarity index measurement system (SSIM) [17], Santiago [18] adopted the statistics of the local variance to evaluate the image quality. The local mean of the

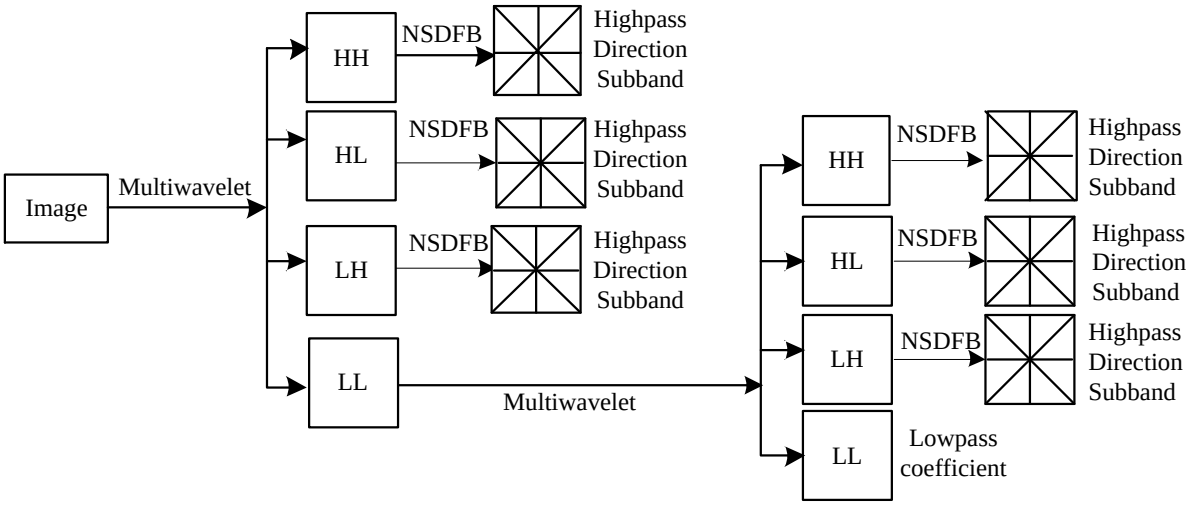

FIGURE 2. MNSDFB decomposition of the image.

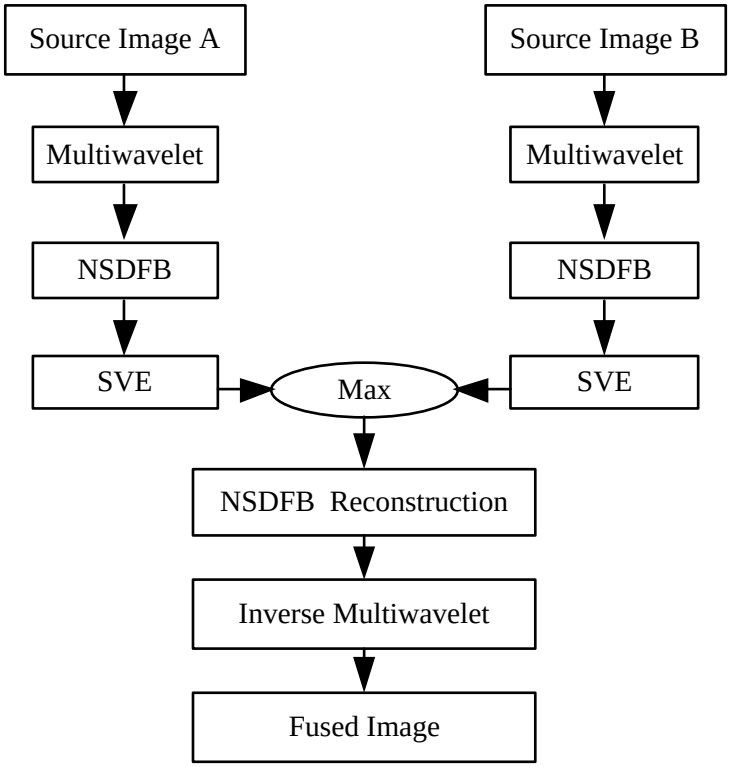

FIGURE 3. Schematic diagram of the proposed fusion method.

MNSDFB coefficient can be expressed as following.

$$\overline{MNSDFB}_{i,j} = \frac{\sum\limits_{p\in\eta_{i,j}} \omega_p MNSDFB_p}{\sum\limits_{p\in\eta_{i,j}} \omega_p} \tag{5}$$

Where ω_p is the weight in the neighborhood of $\eta_{i,j}$. The $MNSDFB^{l,k}(i,j)$ is the coefficient located at the l-th scale and k-th direction subband of the MNSDFB decomposition. In this paper, the Gaussian functions is adopted as the weight to calculate the local mean of the MNSDFB coefficient $MNSDFB^{l,k}(i,j)$. Therefore, the local variance

of $MNSDFB^{l,k}(i,j)$ is defined as:

$$V_{i,j}^{l,k} = \frac{\sum\limits_{p\in\eta_{i,j}} \omega_p (MNSDFB_p^{l,k} - \overline{MNSDFB^{l,k}(i,j)})^2}{\sum\limits_{p\in\eta_{i,j}} \omega_p} \tag{6}$$

The modified local variance takes the absolute values of the second derivatives in the local variance The modified local variance is defined as follows:

$$\begin{aligned} MV^{l,k}(x,y) = &\left|2v^{l,k}(i,j) - v^{l,k}(i-1,jy) - v^{l,k}(i+1,j)\right| \\ &+ \left|2v^{l,k}(i,j) - v^{l,k}(i,j-1) - v^{l,k}(i,j+1)\right| \end{aligned} \tag{7}$$

The sum of the modified local variance energy (SVE) at a point (i,j) is computed as following in a window size of (2M+1)(2N+1) around the center point.

$$SVE^{l,k}(i,j) = \sum_{m=-M}^{M} \sum_{n=-N}^{N} [MV^{l,k}(i+m, j+n)]^2 \tag{8}$$

The decision map can be produced according to the different $SVE^{l,k}(i,j)$ of source images MNSDFB coefficients.

$$Map^{l,k}(i,j) = \begin{Bmatrix} 1, & if & SVE_A^{l,k}(i,j) >= SVE_B^{l,k}(i,j) \\ 0, & if & SVE_A^{l,k}(i,j) < SVE_B^{l,k}(i,j) \end{Bmatrix} \tag{9}$$

Thus, the new fused coefficients $MNSDFB_F^{l,k}(i,j)$ can be merged according to the decision map.

$$MNSDFB_F^{l,k}(i,j) = \begin{Bmatrix} MNSDFB_A^{l,k}(i,j), & if & Map^{l,k}(i,j) = 1 \\ MNSDFB_B^{l,k}(i,j), & if & Map^{l,k}(i,j) = 0 \end{Bmatrix} \tag{10}$$

Where $MNSDFB_A^{l,k}(i,j)$ and $MNSDFB_B^{l,k}(i,j)$ the are the MNSDFB coefficients of the source image A and B, separately. Finally, Fig. 3 shows the block diagram of the proposed fusion method.

TABLE 1. Objective evaluation on the multifocus images fusion results.

Images	Metric	Naidu's	Sudeb's	Kumar's	Proposed
Pepsi	MI	6.5321	7.6071	7.2282	**7.5561**
	$Q^{AB/F}$	0.6709	0.7567	0.7767	**0.7754**
Lab	MI	6.9411	7.7021	7.4774	**8.1199**
	$Q^{AB/F}$	0.6221	0.7178	0.7321	**0.7427**
Disk	MI	5.8289	7.0584	6.6735	**7.6169**
	$Q^{AB/F}$	0.5587	0.6978	0.6950	**0.7165**
Book	MI	6.7423	7.9661	6.3534	**8.4327**
	$Q^{AB/F}$	0.5884	0.7225	0.6566	**0.7206**

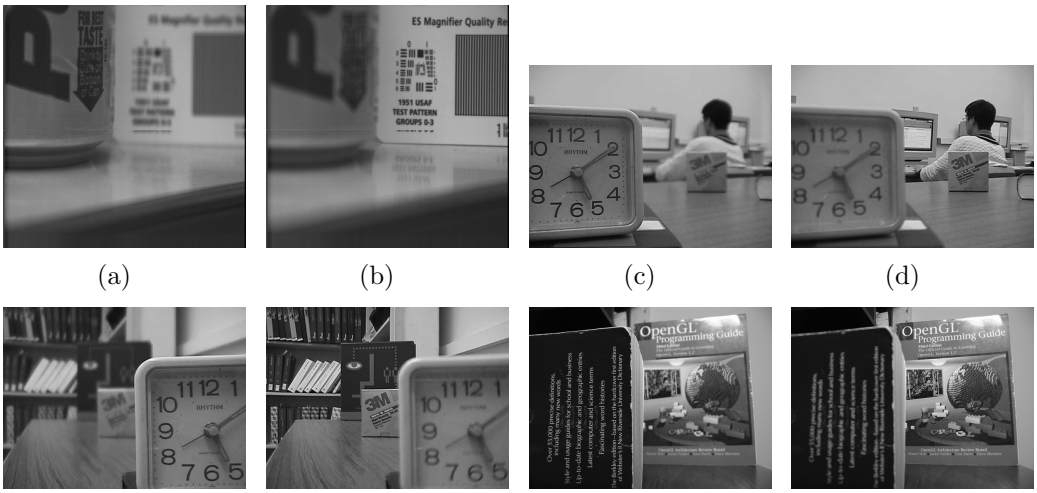

(a) (b) (c) (d)

(e) (f) (g) (h)

FIGURE 4. Source multifocus images for fusion experiments.

4. **Experiments result analysis.** To certify the effectiveness of the presented scheme, the experiments on four pairs of multifocus images have been executed. The source images are shown in the Fig. 4. In the experiments, the proposed method is compared with the multiresolution singular value decomposition (MSVD) method [19], the multiscale geometry analysis method based on NSCT [20], and the cross bilateral filter method [21]. The Naidu's method based on the MSVD used the average and max rules to merge the approximation component and detail component of the one level decomposition of MSVD, separately. In the Sudeb's method based-NSCT, the source images are decomposed by the three scales in which the directions are set to 1, 2, and 4, respectively. The pyramid filter and direction filter are set as pyrex' and vk', respectively. The parameters in the paper [21] are adopted in the Kumar's method based on the cross bilateral filter.

Fig. 5(a)-(d), Fig. 6(a)-(d), Fig. 7(a)-(d), and Fig. 8(a)-(d) demonstrate the fused images by the presented method and the other three methods mentioned above. In order to clearly distinguish the distinction of the fusion results, the difference images between the source image and the fused results fused by the four algorithms are illustrated in the Fig. 5(e)-(h), Fig. 6(e)-(h), Fig. 7(e)-(h), and Fig. 8(e)-(h). If we subtract only one source image from the fused image, the residue image should be close to zero in the well focused part. Hence, the less residual in the residue image means that more information in well focused part of the source images are almost fused into the final image by the fusion method. As shown in Fig.5(e), Fig. 6(e), Fig. 7(e), and Fig. 8(e), Naidu's method produced the most obvious residue information in the four schemes. The difference images in Fig. 5(f) and Fig. 7(f) fused by the Sudeb's algorithm illustrated less residue information than those in Fig. 5(g) and Fig. 7(g) fused by the Kumar's method. On the contrary, Fig. 6(g) and Fig.8(g) by the Kumar's algorithm carry less residue information than Fig. 6(f) and Fig.8(f) by the Sudeb's method do. However, Fig. 5(h), Fig. 6(h), Fig. 7(h), and Fig. 8(h) demonstrate the difference image of near zero in the relevant part. The difference image comparisons show the proposed scheme is most effective to fuse the multifocus images in the four algorithms. For further comparison except for the visual observation above, two objective metrics of the mutual information (MI) [22] and edge information $Q^{AB/F}$ [23] values are introduced to evaluate the four schemes. $Q^{AB/F}$ can measure how much edge information transferred from the source images to the final merged images. MI is adopted to evaluate the amount of information

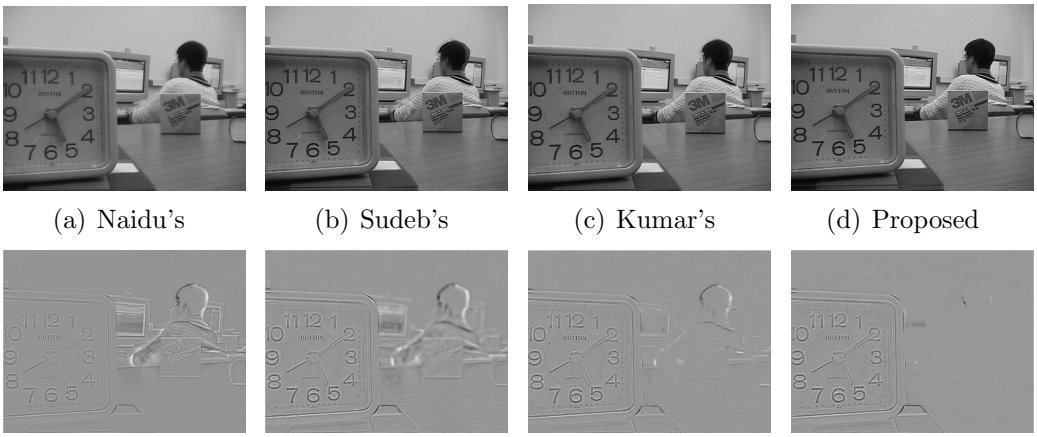

(a) Naidu's (b) Sudeb's (c) Kumar's (d) Proposed

(e) Naidu's (f) Sudeb's (g) Kumar's (h) Proposed

FIGURE 5. Fusion result of Lab images by different methods.

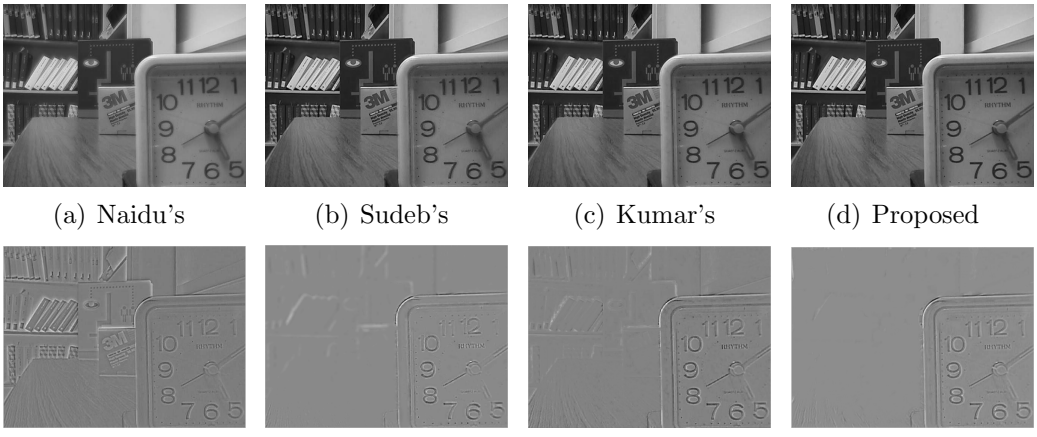

(a) Naidu's (b) Sudeb's (c) Kumar's (d) Proposed

(e) Naidu's (f) Sudeb's (g) Kumar's (h) Proposed

FIGURE 6. Fusion result of 'Disk' images by different methods.

from source images converted into the fusion result. The larger the MI and $Q^{AB/F}$ value are, the better the fusion method is. The MI and $Q^{AB/F}$ values of different fusion schemes are demonstrated in Tab. 1. It is obvious that the MI and $Q^{AB/F}$ values of four fused images by the presented algorithms are larger than those of by the other three schemes. To sum up, just as Tab.1 and Fig. 4-Fig. 7, we may objectively draw the conclusion that the proposed algorithm can preferably extract focus image part and discard the defocused region in the source images according to both visual performance and objective criteria in the four methods. The better performance of the presented approach can be owed to two sides. One is the NSDFBs better directional selectivity and the multiwavelets multiscale, orthogonality, and symmetry characteristic in the proposed MNSDFB transform. On the other hand, the presented sum of local variance energy can competitively separate the focus region from defocused part of source images.

5. **Conclusion.** In this paper, a new multifocus image fusion algorithm is presented. Combining multiwavelet with the nonsubsampled directional filter banks named as MNSDFB transform has been presented in this paper. The proposed MNSDFB transform is not only a 2D image sparse representation method but also a kind of better approximation of image edge. On the other side, the sum of local variance energy is proposed to merge

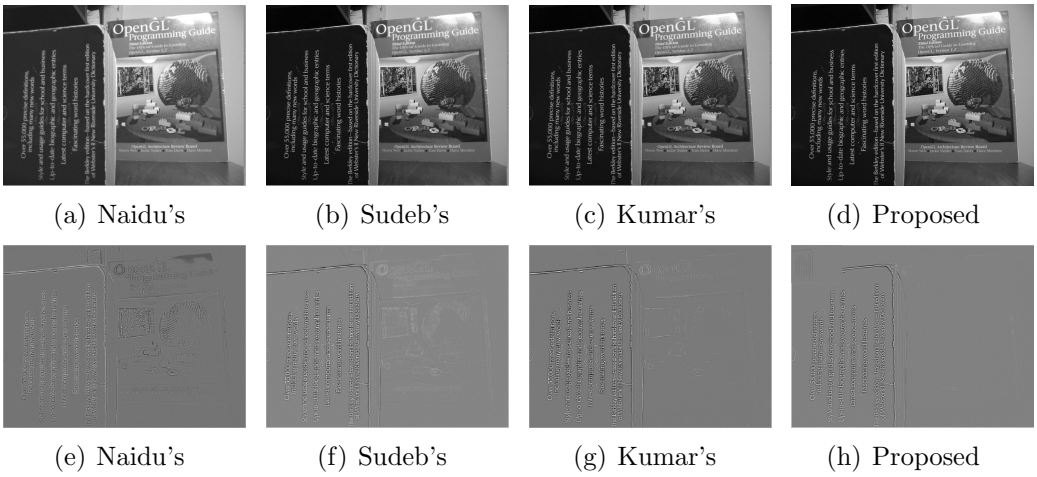

(a) Naidu's (b) Sudeb's (c) Kumar's (d) Proposed

(e) Naidu's (f) Sudeb's (g) Kumar's (h) Proposed

FIGURE 7. Fusion result of 'Book' images by different methods.

the MNSDFB coefficient to final result image. The experiments on four pairs of multifocus demonstrate that the presented scheme is effective in merging the source multifocus image according to the subjective and objective performance valuation.

Acknowledgment. This work was supported in part by the Natural Science Fund of Hebei Province under grants F2013210094 and F2013210109. Source images used in this paper are downloaded from http://www.imagefusion.org. The authors also thank the anonymous referees for their valuable suggestions.

REFERENCES

[1] N. V. Gangapure, S. Banerjee, A. S. Chowdhury, Steerable local frequency based multispectral multifocusimagefusion, *Information fusion*, no.23, pp.99–115, 2015.

[2] E. M. Schetselaar, Fusion by the IHS transform: Should we use cylindrical or spherical coordinates?, *International Journal of Remote Sensing*, vol.19, no.4,pp.759-765,1998

[3] W. Cao, B. Li,Y. Zhang, A remote sensing image fusion method based on PCA transform and wavelet packet transform, *Proc. of Neural Networks and Signal Processing*, pp.II-976–II-981, 2003.

[4] I. Mehra, N. K. Nishchal, Wavelet-based image fusion for securing multiple images through asymmetric keys, *Optics Communications*, no. 335,pp.153–160,2015.

[5] F. Nencini, A. Garzelli, S. Baronti, Remote sensing image fusion using the curvelet transform, *Information fusion*, no.8, pp.143–156, 2007

[6] M.N. Do, M. Vetterli, The contourlet transform: An efficient directional multi-resolution image representation, *IEEE Trans. on Image Process*, no.14,pp. 2091–2106,2005.

[7] A. L. Cunha,J. P. Zhou,M. N. Do, The non-subsampled contourlet transform: Theory, design and applications, *IEEE Trans. on Image Process*, no.15, pp.3089–3101, 2006.

[8] W. Q. Lim, The discrete shearlet transform: A new directional transform and compactly supported shearlet frames, *IEEE Trans. on Image Processing*, vol. 19, no. 5, pp. 1166–1180, 2010.

[9] Y. Yang, S. Huang, J. Gao, Z. Qian, Multi-focus image fusion using an effective discrete wavelet transform based algorithm, *Measurement Science Review*, vol. 14, no.2,pp. 102–108,2014.

[10] K. Liu,L. Guo,J. Chen, Liu Kun, Guo Lei, Chen Jingsong, Contourlet transform for image fusion using cycle spinning, *Journal of Systems Engineering and Electronics*, vol. 22, no.2, pp.353–357,2011.

[11] F. Zhong, Y. Ma, H. F. Li, Multifocus image fusion using focus measure of fractional differential and NSCT, *Pattern recognition and image analysis*,vol. 24, no. 2,pp. 234–242,2014.

[12] X. Liu,Y. Zhou, J. J. Wang, Image fusion based on shearlet transform and regional features, *International Journal of Electronics and Communications*, vol.68, no. 6, pp. 471-477,2014

[13] T. N. T. Goodman, S. L. Lee, Wavelets of multiplicity, *Transactions of the American Mathematical Society*, vol. 342, no.1, pp. 307–324, 1994.

[14] C. H. Zhao, X. Zhong, Q. Dang, L. Zhao, De-noising signal of the quartz flexural accelerometer by multiwavelet shrinkage, *International Journal on Smart Sensing and Intelligent Systems*, vol.6, no.1, pp.191–208, 2013.

[15] L. Zhang,Z. J. Fang, S. Q. Wang,Y. Fan, G. D. Liu, Multiwavelet adaptive denoising method based on genetic algorithm, *Journal of Infrared and Millimeter Waves*, no. 28, pp.77–80,2009.

[16] H. H. Wang, A new Multiwavelet-based approach to image fusion, *Journal of Mathematical Imaging and Vision*, vol. 21,no. 2, pp. 177–192 , 2004.

[17] Z. Wang, A. C. Bovik, H. R. Sheikh, E. P. Simoncelli, Image quality assessment: from error visibility to structural similarity, *IEEE Transactions on Image Processing*,vol. 13, no. 4, pp. 600-612, 2004.

[18] S. Aja-Fernandez, R. San-Jos-Estpar, C. Alberola-Lopez, C. F. Westin, Image quality assessment based on local variance, *Annual International Conference of the IEEE Engineering in Medicine and Biology* , pp. 4815–4818, 2006.

[19] V.P.S. Naidu, Image Fusion technique using Multi-resolution singular Value decomposition, *Defence Science Journal*, vol. 61l, no.5, pp. 479–484,2011.

[20] S. Das, M. K. Kundu, NSCT-based multimodal medical image fusion using pulse-coupled neural network and modified spatial frequency, *Medical and Biological Engineering and Computing*, vol. 50,pp.10, pp.1105–1114,2012.

[21] B. K. Shreyamsha Kumar, Image fusion based on pixel significance using cross bilateral filter. Signal, *Image and Video Processing*, pp. 1–12,2013,doi:10.1007/s11760-013-0556-9.

[22] H. Li,Y. Chai, H. Yin, G. Liu, Multifocus image fusion and denoising scheme based on homogeneity similarity, *Optics Communications*, vol. 285, no. 2,pp. 91–100,2012.

[23] D. Guo, J. W. Yan, X. B. Qu, High quality multifocus image fusion using self-similarity and depth information, *Optics Communications*, vol. 338, no.1, pp. 138–144, 2015.